Supplemental Material for "Scaling Theory for the Fricitionless Unjamming Transition"

Kabir Ramola[1,*] and Bulbul Chakraborty[1,†]

[1]*Martin Fisher School of Physics, Brandeis University, Waltham, MA 02454, USA*

In this document we provide supplemental figures and details of the calculations presented in the main text.

DISTRIBUTION OF AREAS

In Fig. 1 we plot the distribution of the normalized areas $\alpha = a_{g,c}/\sigma_g^2$, obtained from numerical simulations, at different energies E_G. We simulate a system of bidispersed disks, which causes peaks to occur at five values of α corresponding to the different possible combinations of disks within a $z_v = 3$ (ordered) cycle (see ordered structures section). The peak at $\alpha = 1/2$ corresponds to the "disordered divergence" $p_{\rm DO}(\alpha)$ whereas the other five peaks correspond to the "ordered divergences" ($p_{\rm O}(\alpha)$). These peaks ($p_{\rm DO}(\alpha)$ and $p_{\rm O}(\alpha)$) get sharper as $E_G \to 0^+$ and are infinitely sharp at the transition. The rest of the distribution represents the "regular part" $p_{\rm reg}(\alpha)$ that does not have a diverging energy dependence as $E_G \to 0^+$.

TWO POINT DISTRIBUTION $p(\vec{r}_1, \vec{r}_2)$

In this section we develop a diagrammatic expansion for the two point distributions of contact vectors $p(\vec{r}_1, \vec{r}_2)$. From Eq. (10) in the main text we have

$$p(\vec{r}_1, \vec{r}_2) = p(|\vec{r}_1|)p(|\vec{r}_2|)\rho(\theta). \tag{1}$$

along with

$$\int d^2\vec{r}_2 p(\vec{r}_1, \vec{r}_2) = p(\vec{r}_1) = \frac{1}{2\pi} p(|\vec{r}_1|), \tag{2}$$

where $p(\vec{r}_1)$ represents the one point distribution of contact vectors. We then have

$$\rho(\theta) = \frac{p(\vec{r}_1, \vec{r}_2)}{p(|\vec{r}_1|)p(|\vec{r}_2|)}. \tag{3}$$

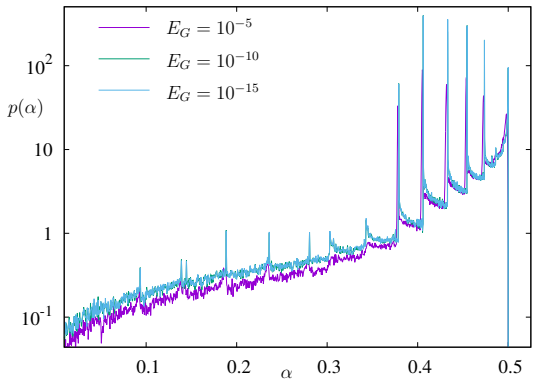

FIG. 1: The distribution of the normalized areas $\alpha = a_{g,c}/\sigma_g^2$, obtained from numerical simulations, at different energies E_G. The plot shows the distribution of α for $N_G = 2048$ bidispersed disks with diameter ratio 1 : 1.4 interacting via harmonic potentials ($\mu = 2$). $\alpha \to 1/2$ corresponds to disks with relative contact angles close to $\pi/2$. The peak at $\alpha = 1/2$ corresponds to the "disordered divergence" $p_{\rm DO}(\alpha)$ whereas the other five peaks correspond to "ordered divergences" ($p_{\rm O}(\alpha)$) arising from $z_v = 3$ cycles (five different possibilities for a bidispersed system, see ordered structures section). The peaks get sharper as $E_G \to 0^+$ and are infinitely sharp at the transition. The rest of the distribution corresponds to the "regular part" $p_{\rm reg}(\alpha)$ and does not have a diverging energy dependence as $E_G \to 0^+$.

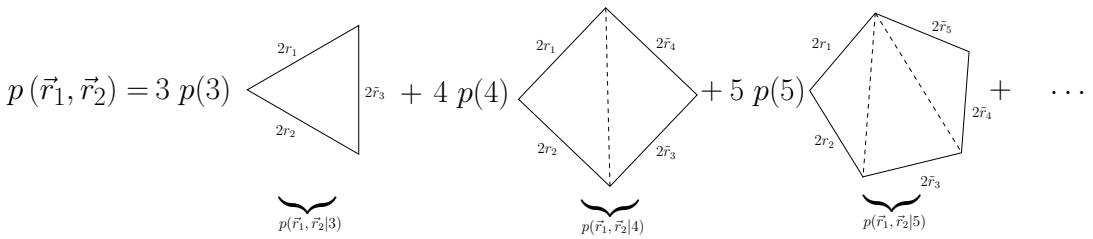

FIG. 2: Diagrams appearing in the expansion for the joint distribution $p(\vec{r}_1,\vec{r}_2)$. The different terms correspond to the minimum cycles with different numbers of sides. The vectors $\tilde{r}$ are integrated over. The terms corresponding to $z_v = 3$ have a fixed length for all the sides as $E_G \to 0^+$, and therefore give rise to $\rho(\theta)$ localized around a single value $\theta = \arcsin\frac{\sqrt{3}}{2}$. The terms corresponding to $z_v > 3$ have unconstrained sides (depicted with dashed lines) and therefore contribute a finite amount to $\rho(\theta)$ at $\theta = \pi/2$.

This function $\rho(\theta)$ therefore encodes the non-trivial correlations between the vectors that arise from the loop constraints. These constraints depend on the number of sides z_v within each cycle. In order to compute the above function $\rho(\theta)$, it is therefore useful to split the joint distribution of the vectors $\vec{r}_1, \vec{r}_2$ into separate categories based on the minimum cycles to which they belong. We do this as follows

$$p(\vec{r}_1,\vec{r}_2) = \underbrace{3p(3)p(\vec{r}_1,\vec{r}_2|3)}_{p(\vec{r}_1,\vec{r}_2,3)} + \underbrace{4p(4)p(\vec{r}_1,\vec{r}_2|4)}_{p(\vec{r}_1,\vec{r}_2,4)} + ... \tag{4}$$

where $p(n)$ is the probability of occurrence of a minimum cycle with $z_v = n$ sides, $p(\vec{r}_1,\vec{r}_2|n)$ is the conditional probability that given a cycle with $z_v = n$ sides two adjacent vectors are $\vec{r}_1, \vec{r}_2$, $p(\vec{r}_1,\vec{r}_2,n)$ represents the joint probability of occurrence of vectors $\vec{r}_1, \vec{r}_2$ together with a cycle of $z_v = n$ sides, and the combinatorial factor accounts for the different ways in which the vectors can be placed within the cycle.

Next, the marginal distribution of these two vectors can be computed from the joint distribution of all the vectors in the cycle as

$$p(\vec{r}_1,\vec{r}_2|n) = \int_0^1 d\tilde{r}_3 \int_0^1 d\tilde{r}_4 ... \int_0^1 d\tilde{r}_n p\left(\vec{r}_1,\vec{r}_2,\vec{\tilde{r}}_3,\vec{\tilde{r}}_4,...\vec{\tilde{r}}_n|n\right), \tag{5}$$

where $p\left(\vec{r}_1,\vec{r}_2,\vec{\tilde{r}}_3,\vec{\tilde{r}}_4,...\vec{\tilde{r}}_n|n\right)$ represents the probability that a given minimum cycle of $z_v = n$ sides has the (ordered) set of vectors $\vec{r}_1,\vec{r}_2,\vec{\tilde{r}}_3,\vec{\tilde{r}}_4,...\vec{\tilde{r}}_n$. We represent this decomposition as a diagrammatic expansion in Fig 2.

In order to proceed further, we next make the crucial assumption that the joint probability of occurence of the n vectors can be represented as a product form, along with the loop constraints. We have

$$p\left(\vec{r}_1,\vec{r}_2,\vec{\tilde{r}}_3,\vec{\tilde{r}}_4,...\vec{\tilde{r}}_n|n\right) = p(\vec{r}_1)p(\vec{r}_2)p(\vec{\tilde{r}}_3)p(\vec{\tilde{r}}_4)...p(\vec{\tilde{r}}_n) \times \delta\left(\vec{r}_1+\vec{r}_2+\vec{\tilde{r}}_3+\vec{\tilde{r}}_4+....\vec{\tilde{r}}_n\right), \tag{6}$$

where each $p(r)$ is chosen from the one point distribution in Eq. (2). This somewhat drastic assumption is justified by the very good agreement between the angular and area distributions obtained from numerical simulations and those obtained by this analysis. This highlights the fact that the crucial correlations in the system arise primarily from these loop constraints. Finally, in order to simplify the analysis further, we assume that all the disks have the same radii (monodisperse), and that each of the contact vector lengths are drawn from a uniform distribution with width $E_G^{1/\mu}$, consistent with the scaling form provided in Eq. (8) in the main text. We have

$$p\left(r = \frac{|\vec{r}|}{\sigma_g}\right) = \frac{1}{{E_G}^{1/\mu}}\Theta\left(r - 1 + {E_G}^{1/\mu}\right)\Theta\left(1-r\right). \tag{7}$$

As the energy of the system approaches zero, the fluctuations in the lengths decrease and $r \sim 1$. From Fig. 2 it is clear that there is a fundamental difference between cycles with $z_v = 3$ and $z_v > 3$ sides. This is because the structures with $z_v = 3$ have a fixed length for all the sides as $E_G \to 0^+$, and therefore give rise to $\rho(\theta)$ localized around a single value $\theta = \arcsin\frac{\sqrt{3}}{2}$. The terms corresponding to $z_v > 3$ have unconstrained sides (as depicted with dashed lines) and therefore contribute a finite amount to $\rho(\theta)$ at $\theta = \pi/2$. We can also explicitly derive the distribution of angles ($p(\sin\theta)$) for the $z_v = 3$ case using the above assumptions, which we detail in the next section.

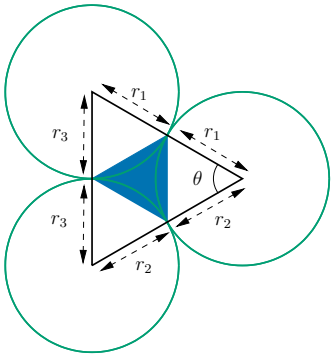

FIG. 3: The three-disk minimum cycle ($z_v = 3$) used to compute the the area distribution in Eq. (9) and angular distribution in Eq. (12). In our analysis we focus only on the case where all the disks have an equal size.

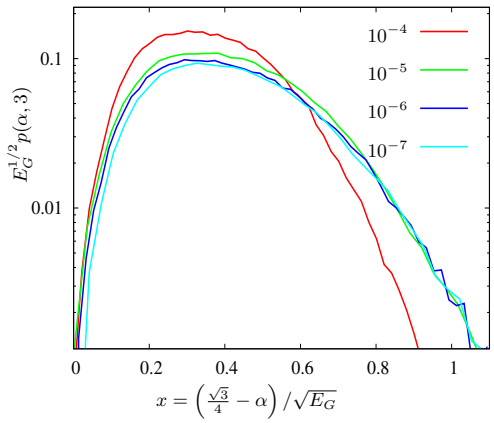

FIG. 4: Scaling collapse of the distribution of areas of the ordered ($z_v = 3$) cycles $p(\alpha, 3)$ obtained from numerical simulations, around the divergence at $\alpha = \sqrt{3}/4$. The plot shows the distribution of α for $N_G = 4096$ disks interacting via harmonic potentials ($\mu = 2$) at different energies. The scaling is consistent with Eq. (4) in the main text.

Ordered Structures ($z_v = 3$)

In this section, we compute the distribution of areas for the $z_v = 3$ cycles and provide the scaling form for the "ordered divergence" mentioned in the main text. From Fig. 3 it is straightforward to compute

$$\sin\theta = \frac{\sqrt{4r_1^2r_2^2 - (r_1^2 + r_2^2 - r_3^2)}}{2r_1r_2}. \tag{8}$$

Using the above expression, the distribution of areas for the $z_v = 3$ cycles can be computed as

$$p(\alpha, 3) = \int_0^1 dr_1 \int_0^1 dr_2 \int_0^1 dr_3 \; p(r_1)p(r_2)p(r_3) \; \delta\left(\alpha - \frac{\sqrt{4r_1^2r_2^2 - (r_1^2 + r_2^2 - r_3^2)}}{4}\right). \tag{9}$$

Next, replacing $p(r)$ with the uniform distributions in Eq. (7) leads to the following scaling form for the ordered divergence in the distribution of areas

$$p(\alpha, 3) = \frac{1}{{E_G}^{1/\mu}} \mathcal{P}_{\rm O}\left(\frac{\alpha - \frac{\sqrt{3}}{4}}{{E_G}^{1/\mu}}\right), \tag{10}$$

which is Eq. (4) in the main text. In Fig. 4 we plot the scaling collapse of the distribution $p(\alpha, 3)$ obtained from numerical simulations, around the divergence at $\alpha = \sqrt{3}/4$. The scaling is consistent with the above analysis and

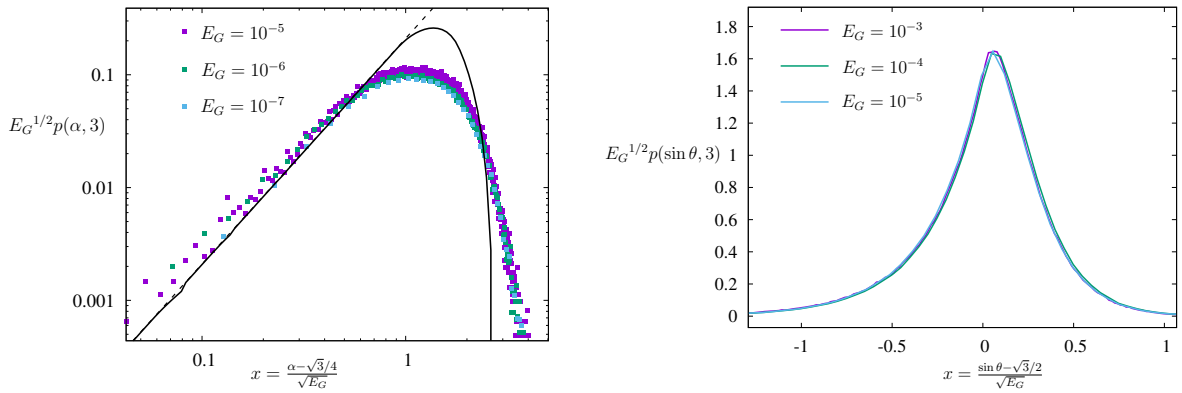

FIG. 5: **(Left)** Scaling collapse of the distribution of contact areas of the $z_v = 3$ cycles obtained from numerical simulations along with the prediction from the theory. The plot shows the distribution of α for $N_G = 4096$ bidispersed disks interacting via harmonic potentials ($\mu = 2$). The bold line represents the theoretical distribution obtained by numerically integrating Eq. (9) using a uniform distribution of contact vector lengths given in Eq. (7) with $\mu = 2$. The dashed line has a slope 2. **(Right)** Scaling collapse of the theoretical distribution of $p(\sin\theta, 3)$ obtained by numerically integrating Eq. (12) for $\mu = 2$. The distribution obeys the scaling form provided in Eq. (13).

with Eq. (4) in the main text. The scaling behaviour of the distribution obtained from our theoretical analysis is illustrated in Fig. 5 where we plot the distribution of areas computed numerically using Eq. (9), along with the distributions obtained from numerical simulations. We find a good agreement between the distributions in the limit $\alpha \to \sqrt{3}/4$. The scaling function has the following behaviour

$$\mathcal{P}_{\rm O}(x) \sim x^2 \quad \text{for} \quad x \to 0. \tag{11}$$

We note that in our analysis we have only focussed on monodispersed disks. The generalization to the polydisperse case involves all combinations of disks that can produce a $z_v = 3$ cycle. For the bidispersed case with diameter ratio $1 : 1.4$ that we simulate, the peaks in the area distribution occur at $\alpha = \sqrt{3}/4 = 0.433013$ (for equal sized disks), $0.406116, 0.45453, 0.378775$ and 0.473803 [1] (see Fig. 1). The scaling analysis for each of these cases remains the same.

Similarly, using the product assumption in Eq. (6), the distribution of the angles $p(\sin\theta)$ for finite energies corresponding to the $z_v = 3$ cycles can be explicitly computed as

$$p(\sin\theta, 3) = \int_0^1 dr_1 \int_0^1 dr_2 \int_0^1 dr_3 \; p(r_1)p(r_2)p(r_3) \; \delta\left(\sin\theta - \frac{\sqrt{4r_1^2 r_2^2 - (r_1^2 + r_2^2 - r_3^2)}}{2r_1 r_2}\right). \tag{12}$$

Next, replacing $p(r)$ with the uniform distributions in Eq. (7) we find the following scaling form for the angular distribution

$$p(\sin\theta, 3) = \frac{1}{{E_G}^{1/\mu}} \mathcal{P}_\theta\left(\frac{\sin\theta - \frac{\sqrt{3}}{2}}{{E_G}^{1/\mu}}\right). \tag{13}$$

This behaviour is illustrated in Fig. 5 where we plot the angular distributions computed numerically using Eq. (12) for $\mu = 2$.

Disordered Divergence: $p_{\rm DO}(\alpha)$

In this section we derive an expression for the disordered divergence $p_{\rm DO}(\alpha)$ in the distribution of areas. We begin by assuming a product form for the joint distribution of contact vectors

$$p(\vec{r}_1, \vec{r}_2) = \frac{1}{2\pi} p(r_1)p(r_2). \tag{14}$$

In the above decomposition, we have assumed a uniform distribution for $\rho(\theta)$ in the region $[0, 2\pi]$. This assumption is justified since we are interested in the distribution close to $\theta \sim \pi/2$. The analysis presented in this section can easily

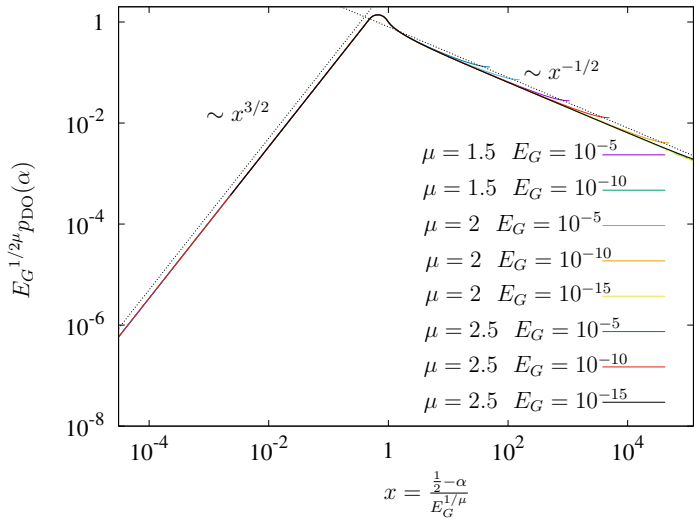

FIG. 6: Scaling collapse of the theoretical distribution of $p_{\rm DO}(\alpha)$ obtained from Eqs. (19) and (21) for different repulsive potentials $\mu = 1.5, 2$ and 2.5 at varying global energies. The distribution obeys the scaling form provided in Eq. (2) in the main text. The scaling function has the limiting behaviours announced in Eq. (3) in the main text.

be generalized to smaller ranges of θ. We have checked that the scaling features of the distribution near the transition are unchanged by extending the range of θ. We then have

$$\rho(\sin\theta) = \frac{1}{2\pi}\frac{1}{\sqrt{1-\sin^2\theta}}. \tag{15}$$

Next, from Eq. (9) in the main text we have the following equation for the distribution of the areas

$$p(\alpha) = \int_0^1 dr_1 \int_0^1 dr_2 \int_0^1 d\sin\theta \; p(r_1)p(r_2)\rho(\sin\theta) \; \delta\left(\frac{1}{2}r_1 r_2 \sin\theta - \alpha\right). \tag{16}$$

Once again to simplify the analysis, we replace the one point distribution of contact vector lengths $p(r)$ by the uniform distribution in Eq. (7). Finally, performing the integral over $\sin\theta$ we arrive at the following expression for the distribution of areas

$$p_{\rm DO}\left(\alpha\right) = \frac{4}{\pi {E_G}^{2/\mu}} \int_{1-{E_G}^{1/\mu}}^1 \int_{1-{E_G}^{1/\mu}}^1 \frac{\Theta(xy-2\alpha)}{\sqrt{x^2y^2-4\alpha^2}} dxdy. \tag{17}$$

In order to perform this computation we compute the simpler indefinite integral defined as

$$S_{\rm DO}(\alpha, x, y) = \int\int \frac{1}{\sqrt{x^2y^2-4\alpha^2}} dxdy. \tag{18}$$

This does not explicitly contain the Θ function. We can account for the $\Theta(xy-2\alpha)$ constraint by breaking the definite integral into regions depending on the value of α. The definite integral can then be expressed as combinations of the above indefinite integral. We have

$$p_{\rm DO}(\alpha) = \frac{4}{\pi {E_G}^{2/\mu}} \left(S_{\rm DO}(\alpha,1,1) - S_{\rm DO}(\alpha,1,1-{E_G}^{1/\mu}) - S_{\rm DO}(\alpha,1-{E_G}^{1/\mu},1) + S_{\rm DO}(\alpha,1-{E_G}^{1/\mu},1-{E_G}^{1/\mu})\right). \tag{19}$$

Explicit expression for $S_{\rm DO}(\alpha, x, y)$

We derive below an exact expression for the above indefinite integral $S_{\rm DO}(\alpha, x, y)$. First, performing the integral over x we arrive at

$$S_{\rm DO}(\alpha, x, y) = \int \frac{\log\left(y\sqrt{x^2y^2-4\alpha^2} + xy^2\right)}{y} dy. \tag{20}$$

Next, the integral with respect to y can be performed exactly. After some algebraic simplifications (using Mathematica), the explicit expression is

$$S_{\rm DO}(\alpha,x,y) = -\frac{1}{2}{\rm Li}_2\left(\frac{2\alpha^2}{2\alpha^2 - xy\left(xy+\sqrt{x^2y^2-4\alpha^2}\right)}\right) - \frac{1}{2}\log^2\left(\sqrt{x^2y^2-4\alpha^2}+xy\right) + \log(xy)\log\left(\sqrt{x^2y^2-4\alpha^2}+xy\right)$$
$$+ \log(2)\log\left(\frac{\sqrt{x^2y^2-4\alpha^2}}{x}+y\right) + \frac{1}{2}\log(\alpha)\log\left(\frac{\alpha}{x^2}\right) + \frac{1}{2}\log^2(y) - \frac{\pi^2}{8} - \frac{1}{2}\log^2(2), \quad (21)$$

where ${\rm Li}_2$ is the Polylogarithm function. Although the above expression is not explicitly symmetric under the $(x,y)\to(y,x)$ transformation, it is easy to see that the expression $p_{\rm DO}(\alpha)$ preserves this symmetry. Using Eq. (21) it is straightforward to show (for example, using Mathematica) that the function $p_{\rm DO}(\alpha)$ given in Eq. (19) has the asymptotic behaviours mentioned in the scaling form in Eq. (3) in the main text.

In Fig. 6 we show the scaling collapse of the theoretical distribution $p_{\rm DO}(\alpha)$ obtained from Eqs. (19) and (21) for different repulsive potentials $\mu = 1.5, 2$ and 2.5. The distribution obeys the scaling form provided in Eq. (2) in the main text. The scaling function has the limiting behaviours announced in Eq. (3) in the main text.

* Electronic address: kramola@brandeis.edu
† Electronic address: bulbul@brandeis.edu

[1] K. Ramola and B. Chakraborty, J. Stat. Mech. 114002 (2016).